ARL-TR-10302 • Mar 2026

Mechanical Stability of Bonded Dissimilar Materials When Subjected to Thermal Stresses

by Efraín Hernández-Rivera, Matthew C. Guziewski, S. Gary Hirsch, and Brady Butler

NOTICES

Disclaimers

ARL-TR-10302 ● Mar 2026

Mechanical Stability of Bonded Dissimilar Materials When Subjected to Thermal Stresses

Efraín Hernández-Rivera, Matthew C. Guziewski, S. Gary Hirsch, and Brady Butler
DEVCOM Army Research Laboratory

REPORT DOCUMENTATION PAGE

1. REPORT DATE	2. REPORT TYPE	3. DATES COVERED	
		START DATE	END DATE
March 2026	Technical Report	October 1, 2023	September 30, 2025

4. TITLE AND SUBTITLE
Mechanical Stability of Bonded Dissimilar Materials When Subjected to Thermal Stresses

5a. CONTRACT NUMBER	5b. GRANT NUMBER	5c. PROGRAM ELEMENT NUMBER

5d. PROJECT NUMBER	5e. TASK NUMBER	5f. WORK UNIT NUMBER
AH80		

6. AUTHOR(S)
Efraín Hernández-Rivera, Matthew C. Guziewski, S. Gary Hirsch, and Brady Butler

7. PERFORMING ORGANIZATION NAME(S) AND ADDRESS(ES)	8. PERFORMING ORGANIZATION REPORT NUMBER
DEVCOM Army Research Laboratory ATTN: FCDD-RLA-MB Aberdeen Proving Ground, MD 21005-5066	ARL-TR-10302

9. SPONSORING/MONITORING AGENCY NAME(S) AND ADDRESS(ES)	10. SPONSOR/MONITOR'S ACRONYM(S)	11. SPONSOR/MONITOR'S REPORT NUMBER(S)

12. DISTRIBUTION/AVAILABILITY STATEMENT
DISTRIBUTION STATEMENT A. Approved for public release: distribution unlimited.

13. SUPPLEMENTARY NOTES
ORCID(s): Efraín Hernández-Rivera, 0000-0002-7855-1027; Matthew C. Guziewski, 0000-0002-5761-720X ; Brady G. Butler, 0000-0002-7677-9685

14. ABSTRACT
The joining of dissimilar materials, such as ceramic-metal composites, for high-temperature applications is often limited by the large residual stresses induced by a mismatch in material properties during thermal processing. In this work, a closed-form thermoelastic model is extended to analyze the 2-D stress state in a bonded silicon carbide and Ti-6Al-4V bilayer system. A key aspect of the analysis is the implementation of a composite failure metric, which applies a maximum principal stress criterion for the brittle ceramic and a von Mises stress criterion for the ductile metal, providing a more realistic assessment of failure risk across the entire component. The model's predictions show qualitative agreement with a finite element simulation, confirming that maximum stresses are concentrated at the free edge and the material interface. Parametric studies demonstrate a linear dependence of maximum stress on the processing temperature change and a nonlinear relationship with the layer thickness ratio. The findings establish the closed-form model as an efficient and valuable design tool for optimizing layer geometries and thermal processing conditions to mitigate residual stresses and enhance the mechanical reliability of ceramic-metal composites in extreme environments.

15. SUBJECT TERMS
bonding, closed-form, dissimilar material, finite element, Sciences of Extreme Materials, stress, thermoelasticity

16. SECURITY CLASSIFICATION OF:			17. LIMITATION OF ABSTRACT	18. NUMBER OF PAGES
a. REPORT	b. ABSTRACT	C. THIS PAGE		
UNCLASSIFIED	UNCLASSIFIED	UNCLASSIFIED	UU	32

19a. NAME OF RESPONSIBLE PERSON	19b. PHONE NUMBER *(Include area code)*
Efraín Hernández-Rivera	(520) 691-4849

STANDARD FORM 298 (REV. 5/2020)
Prescribed by ANSI Std. Z39.18

Contents

List of Figures

List of Tables

Acknowledgments

We would like to acknowledge Dr. Alberto Torres for a very exhaustive review of this manuscript.

1. Introduction

Large heat fluxes and loads are characteristics of sustained high velocity flights, which vary not only locally on the vehicle but also during the mission stage. Few, if any, material systems are able to perform at high levels for sustained high speed flights, often requiring complex cooling strategies. This can be critical for components like leading edges, where preferred designs minimizing drag lead to surface temperatures in excess of 2,400 K. When designing for operation under such extreme conditions, these material challenges are often addressed via refractory carbides or borides, or carbon/carbon (C/C) composites; however, these materials are susceptible to severe oxidation and catastrophic failure (cracking) under the elevated thermal gradients they experience.[1] While leading edges can partially manage heat through radiation, the larger vehicle body must rely on advanced materials to withstand prolonged thermal loads. Structural components often use high strength-to-weight ratio materials such as titanium (Ti) alloys. However, high-temperature tolerant materials (e.g., carbon-carbon composites [CCCs] or ceramic matrix composites [CMCs]) are necessary for the most extreme temperatures found at nose tips. The operational envelope of these composites is ultimately limited by factors such as high-temperature oxidation and the formation of microcracks driven by intense thermal gradients, which compromise their structural integrity. These challenges motivate the development of new material systems, often composed of dissimilar material classes like metallic ceramic composites (MCC).

A major challenge in using MCCs is the non-trivial task of joining two materials with drastically different properties (e.g., coefficient of thermal expansion [CTE]). For instance, the CTE characterizes a material's rate of expansion and/or contraction when undergoing heating/cooling. When materials of significantly different CTEs are bonded and subjected to a temperature change, the mismatch in the expansion and/or contraction results in residual thermal strains. One such system is silicon carbide (SiC)/Ti, which aims to leverage the high-temperature resistance strength of SiC and Ti, respectively, making it a promising candidate for applications operating under extreme thermal conditions. Other relevant research areas of applications where SiC/Ti joining include nuclear energy applications in which current efforts attempt to join SiC to SiC for fuel cladding tubes.[2] Unfortunately, joining these two material classes is non-trivial due to poor wettability and differences in thermomechanical properties.

Conventional approaches for joining include diffusion bonding of SiC onto foils for a variety of different metallic systems,[2,3] solid-state reaction of SiC/titanium carbide (TiC) tape cast ribbons,[4] and brazing where a filler metal layer is brought to its melting temperature, joining the base materials.[5] Jung et al.[2] found that adding Si to the Ti film helps increase joining strength as the free Si enables reaction bonding of the SiC. Promising results were shown by Henager et al.,[4] finding that shear strength can be improved using SiC/TiC tape cast ribbons, exceeding that of SiC/SiC composites. It has been shown when joining SiC, processing conditions are critical to the bond's mechanical properties; long hold times lead to thicker reaction layers and increased CTE mismatch.[5] Furthermore, these joints become weaker at higher temperatures due to the softening of the filler alloy and the formation of large residual stresses upon cooling from the mismatch in CTE may lead to reduced strength. These additional stresses may limit the maximum allowable flaw size of the ceramic to the typical pores size (a few micrometers).[6] Lastly, these bonds are weaker near edges due to free edge effects, resulting in interfacial peeling (i.e., normal to the inteface) and shear stresses form locally.[7,8]

The studies herein focus on using metallic laminates as the joining medium between two ceramics, i.e., a multilayered system featuring thin metallic interlayers. For relevant applications, joining thicker materials would be required (as shown in Figure 1a), resulting in a composite system with critical potential to failure. To fully understand how differences in material thermomechanical properties compromise the mechanical stability of bonded dissimilar material upon cooling, a simple thermoelasticity model developed by Hsueh et al.[9–12] was adopted. We demonstrate how the Hsueh model was extended to predict a full 2-D stress profile by coupling functional forms proposed by Bao et al.,[13] similar to the recent work by Pelz et al.[14]

2. Mathematical Model Formulation

To understand the residual stresses that form due to differences in material properties (e.g., CTEs), we employ the macroscale model developed by Hsueh,[9,12] in which the mechanical response is decomposed into uniform and bending strains. A closed form (CF) solution for in-plane stress (parallel to the interface) within the layered system can be derived by balancing force and moment in the system, and is given by

$$\sigma_n = E\left(\varepsilon_u + \varepsilon_b + \varepsilon_{th}\right) = E\left(\varepsilon_u + \frac{z - z_b}{\mathcal{R}} - \alpha\Delta T\right) \tag{1}$$

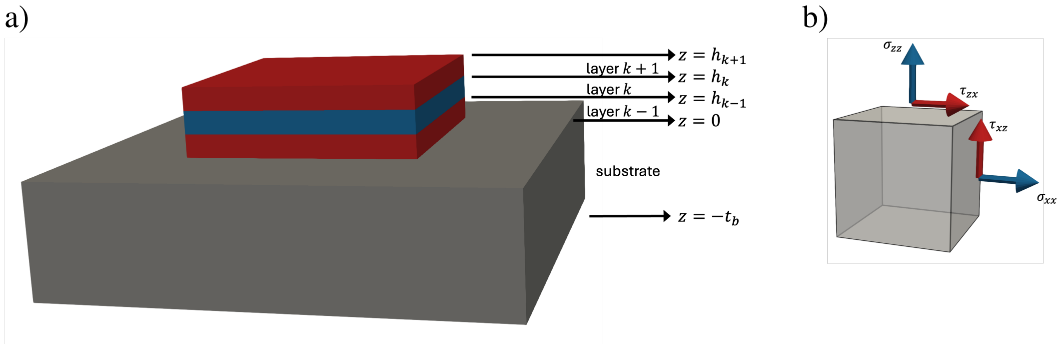

Figure 1. Schematics for the computational domain show, a) a multilayered system and coordinate framework used in the analysis, and b) showing the expected stress states.

where E is the Young's modulus for the i^{th} layer, ε_u is the uniform strain component, $\varepsilon_b = (z - z_b)/\mathcal{R}$ is the bending strain component, and $\varepsilon_{th} = -\alpha_i \Delta T$ is the thermal strain component. For the bending strain, z_b is the bending axis (i.e., height at which the bending strain is zero), and $\mathcal{R}$ is the radius of the curvature of the layered system. For the thermal strain, α_i is the i^{th} layer coefficient of thermal expansion and $\Delta T = T - T_0$ is the change in temperature from the reference temperature T_0.

Following Hsueh,[9] the uniform strain component is

$$\varepsilon_u = \left(\frac{E_s t_s \alpha_s + \sum_{i=1}^{n} E_i t_i \alpha_i}{E_s t_s + \sum_{i=1}^{n} E_i t_i} \right) \Delta T, \tag{2}$$

and the parameters for the bending strain are

$$z_b = \frac{-E_s t_s^2 + \sum_{i=1}^{n} E_i t_i (2h_{i-1} + t_i)}{2\left(E_s t_s + \sum_{i=1}^{n} E_i t_i\right)}, \tag{3}$$

and

$$\mathcal{R} = \frac{E_s t_s^2 (2t_s + 3z_b) + \sum_{i=1}^{n} E_i t_i \left[6h_{i-1}^2 + 6h_{i-1} t_i + 2t_i^2 - 3z_b(2h_{i-1} + t_i)\right]}{3\left[E_s(\varepsilon_u - \alpha_s \Delta T) t_s^2 - \sum_{i=1}^{n} E_i t_i (\varepsilon_u - \alpha_i \Delta T)(2h_{i-1} + t_i)\right]} \tag{4}$$

where the subscript s stands for substrate, n is the number of layers, and t_i and h_i are the i^{th} layer's thickness and global height, respectively. To derive these parameters, the following boundary conditions must be satisfied:[9,10]

1. resultant force due to ε_u is zero,
2. resultant force due to ε_b is zero,
3. resultant bending moment due to stresses (see Equation 1) is zero.

Lastly, the height and thickness are related by

$$h_i = \sum_{j=1}^{i} t_j, \qquad i \in [1, n], \tag{5}$$

with the condition that for the first layer ($i = 1$) $h_0 = 0$, as shown in Figure 1a. When the multilayer system is placed on a substrate, the domain's global coordinates system is $z = [-t_s, h_{n+1}]$.

The model assumes a free-surface condition, requiring the use of imaginary applied tractions at the free edge, which induces the interfacial peeling (σ_{ip}) and shear (τ) stresses. This is achieved by assuming the stress field σ_n exists along the laminate interfaces and applying tractions of the same magnitude but opposite direction (i.e., $-\sigma_n$) along the corresponding locations, resulting in stress-free edges.[11] At the base of each layer i (i.e., $z = h_{i-1}$), the resulting peeling moment and shear force are in equilibrium with the corresponding counteracting imaginary applied tractions, which yields the peeling moment per unit length

$$M_k = -\sum_{i=k}^{n} \int_{h_{i-1}}^{h_i} \sigma_i \cdot (z - h_{k-1}) dz \tag{6}$$

and the shear force per unit length

$$V_k = -\sum_{i=k}^{n} \int_{h_{i-1}}^{h_i} \sigma_i dz \tag{7}$$

where $k \in [1, n]$. Note that these integral forms avoid complications related to the singularity problem that would arise at the edge region. To derive forms of these components that vary through the thickness (i.e., are a function of height, $f(z)$), we note that the integrals can be separated into the region contained within a layer k and above ($i = [k, \ldots, n]$). With this, it can be shown (see the Appendix) that Equations 6 and 7 can be expressed as

$$M_k(z) = -\sum_{i=k}^{n} E_i \left[\left(\varepsilon_u + \frac{z - z_b}{\mathcal{R}} - \alpha_i \Delta T \right) \frac{(z - h_{k-1})^2}{2} - \frac{(z - h_{k-1})^3}{6\mathcal{R}} \right] \Bigg|_{\mathrm{T}_i} \tag{8}$$

and

$$V_k(z) = -\frac{\mathcal{R} E_k}{2} \left(\varepsilon_u + \frac{z - z_b}{\mathcal{R}} - \alpha_k \Delta T \right)^2 \Bigg|_{\mathrm{T}_k} + V_{k+1}^e \tag{9}$$

where $\mathrm{T}_i \equiv \{h_{i-1}, h_i\}$ denotes the i^{th} layer domain (i.e., thickness) and the exact (CF) solution for the shear force is given by (see Hsueh[11] Equation 7)

$$V_{k+1}^e = -\sum_{i=k+1}^{n} E_i t_i \left[\varepsilon_u - \alpha_i \Delta T + \frac{1}{\mathcal{R}} \left(\frac{t_i}{2} + h_{i-1} - z_b \right) \right] \tag{10}$$

The following observation involving layer domain T_i where $i = k$, i.e., the layer on which z is locally defined, is noted. Given that the Hsueh model is formulated such that the residual stress contribution is attributed to layers above the layer in consideration, integrating the thickness domain is defined as $\{\mathrm{T}_i \in \mathbb{R} : z \leq z' \leq h_i\}$. This is similar to estimating the remaining water in a draining tank reservoir of height H where the integral is bounded by $\{z, H\}$.

These CF solutions yield the stress components at the free surface, and in turn are maximum at the edges. Following the work by Pelz et al.,[14] we derive functions for the in-plane stress distribution axially across the sample while maintaining this boundary condition. We begin by relating the interfacial peeling and shear stresses to the corresponding moment and force

$$M_{k,\max} = \int_0^{x_0} \sigma_z \cdot \ x dx \tag{11}$$

and

$$V_{k,\max} = \int_0^{x_0} \tau dx \tag{12}$$

where

$$x = \begin{cases} 0, & \text{free edge} \\ x_0, & \text{location of zero stress.} \end{cases}$$

While Hsueh et al.[11,12] used finite elements (FE) to determine these stresses, we rely on an analytical definition proposed by Bao et al.[13] who provides a functional form for the normal interfacial stress

$$\sigma(x) = D\left[(L-x)^{m-1} - (L-x_t)^{m-1}\right] \tag{13}$$

and a shear stress within laminates

$$\tau(x) = \tau_0 \left(\frac{L-x}{L}\right)^m \tag{14}$$

where $2L$ is the layer width, τ_0, m and D are material properties, and x_t is the transition distance (i.e., threshold at which the normal stress transitions from compressive to tensile) and is given by

$$x_t = L \cdot \left(1 - \frac{1}{m^{1/(m-1)}}\right). \tag{15}$$

Note that these functional forms are altered to account for discrepancies between the Hsueh and Bao model's boundary conditions (i.e., location of the free edge), as shown in Figure 2. The Bao formulation yields maximize stresses at $x = L$, where the free edge location is defined. However, Hsueh framework defines the free edge is at $x = 0$. Figures 2a and b show the functional forms used in this work maximize at $x = 0$ and minimize at $x = L$, as expected to agree with the Hsueh model. Further, Figure 2c shows that the transition distance used in this work and by Bao asymptotically approach zero and one, respectively. A critical parameter for these analytical forms is the material-dependent exponent m. Bao et al. suggests that $\{m \in \mathbb{R} : 4 \leq m \leq 6\}$ for ceramic laminates; however, no guidance is provided for metallic systems. From Figure 2b, it is clear that a higher m results in a sharper decrease in shearing stress as a function to distance from the free edge. This is a reasonable assumption for ceramics that have comparatively immobile dislocations, limiting the extent of stress relaxation. Therefore, we assume $\{m \in \mathbb{R} : 3/2 \leq m \leq 3\}$ for metals, which are understood to plastically deform under shear stress due to mobile dislocation networks. However, the normalized shear stress material constant for ceramics (larger m) is expected to have a larger value, as shown in Figure 2d. Metals readily deform plastically, which relieves residual stresses, reduces stress concentrations, and minimizes stress gradients toward uniformity.

To determine the D and τ_0 material properties, Equations 13 and 14 are substituted into Equations 11 and 12, resulting in the following expressions for the axial in-plane stress

$$\sigma_{z|k}(x) = -\frac{2m(m+1) \cdot \ M_{k,\max} \cdot \left[(L-x)^{m-1} - (L-x_t)^{m-1}\right]}{2(L-x_0)^m \cdot (L+mx_0) + m(m+1) \cdot (L-x_t)^{m-1} x_0^2 - 2L^{m+1}} \tag{16}$$

and shear stress

$$\tau_{z|k}(x) = -\frac{(m+1)L^m V_{k,\max}}{L^{m+1} - (L-x_0)^{m+1}} \left(\frac{L-x}{L}\right)^m . \tag{17}$$

Given that we are considering a 2-D domain, we can assume plane stresses (see Figure 1b), which result in the following expression for the stress tensor

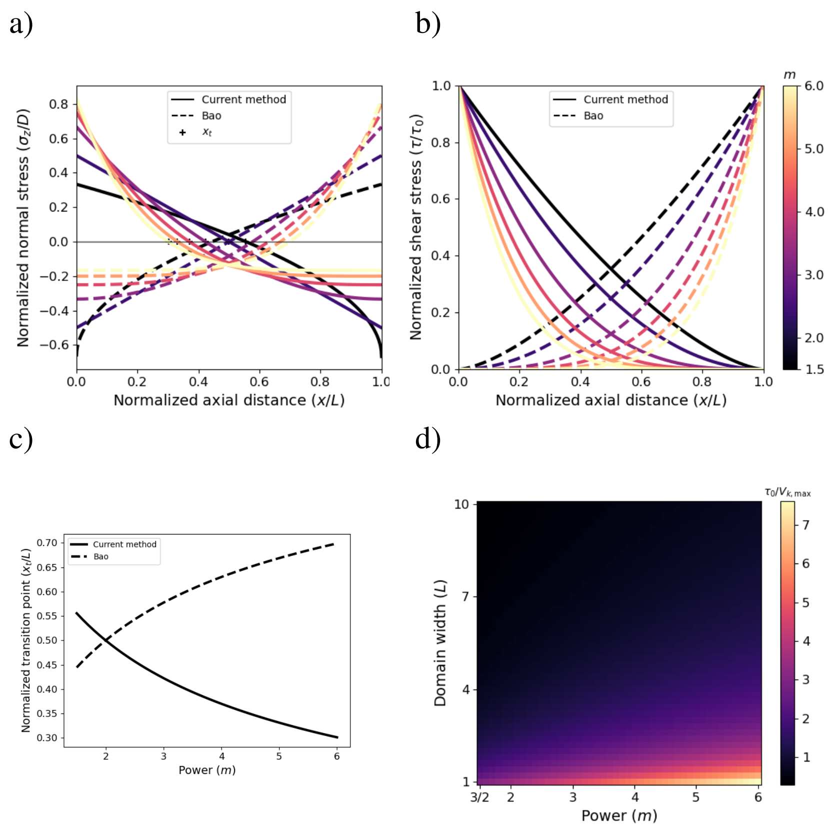

Figure 2. Comparison between functional forms for the a) Normalized normal stress, b) normalized shear stress, c) transition distance, and d) normalized maximum shear stress as a function of material property (m) and width (L).

$$\boldsymbol{\sigma} = \begin{bmatrix} \sigma_{xx} & \sigma_{xy} & \sigma_{xz} \\ \sigma_{yx} & \sigma_{yy} & \sigma_{yz} \\ \sigma_{zx} & \sigma_{zy} & \sigma_{zz} \end{bmatrix} = \begin{bmatrix} \sigma_{xx} & 0 & \sigma_{xz} \\ 0 & 0 & 0 \\ \sigma_{zx} & 0 & \sigma_{zz} \end{bmatrix} = \begin{bmatrix} \sigma_n(z) & \tau_{z|k}(x) \\ \tau_{z|k}(x) & \sigma_{z|k}(x) \end{bmatrix} \tag{18}$$

where these stress components are given by Equations 1, 16, and 17, respectively. The plane stress assumption is accurate for thin samples (i.e., in depth along the y-axis for our purposes); however, this formulation provides a good first-order approximation to the expected mechanical response. This formulation is used to analyze the effects of thermal processing the dissimilar SiC and Ti-6Al-4V (Ti64) material system in the following sections.

3. Bilayer Analysis

As a demonstration, we consider the SiC–Ti64 bilayer system, whose material properties are given in Table 1. First, we consider a bilayer system of equally thick layers ($t = 12.7$ mm) with Ti64 laid on top of SiC (SiC/Ti64). In this example, we allow the material parameter m to remain constant across the material, i.e., $m_{\mathrm{Ti64}} = m_{\mathrm{SiC}} = 6$. The maximum in-plane, peeling, and shear stresses at every height location [i.e., $\max(\boldsymbol{\sigma}(z))$] are shown in Figure 3 for both the a) CF and b) FE models. While the CF does not identically reproduce the FE results, there are several features of agreement. For instance, both models agree that the peeling stress initially increases in the SiC layer and then sharply decreases as it nears the interface, eventually transitioning into a compressive state in the metallic layer. Furthermore, the shear stresses are observed to be slightly compressive in the SiC layer as it approaches the interface and abruptly increase as it nears the interface, followed by a asymptotic decrease to zero at the top of the Ti64 layer. However, it is of note that the asymptotic behavior of the in-plane stress found in the FE results is not captured by the CF model. Nonetheless, the CF model does capture the correct direction (compressive for SiC and tensile for Ti64) and approximates the correct magnitudes at the interface (where failure is expected)

$$\min(\sigma_{\mathrm{SiC}}^{\mathrm{in-plane}}) = \begin{cases} -596.20 \text{ MPa}, & \text{FE} \\ -595.65 \text{ MPa}, & \text{CF} \end{cases}$$

and

$$\max(\sigma_{\mathrm{Ti64}}^{\mathrm{in-plane}}) = \begin{cases} 425.99\ \mathrm{MPa}, & \text{FE} \\ 378.10\ \mathrm{MPa}, & \text{CF} \end{cases}.$$

Another aspect to note is that the peeling stress for the FE model has a distinguishable discontinuity while the CF shows a cusp (singularity) at the interface. While it is less pronounced in the FE model, a discontinuity is observed, even though it is finely meshed (element discretization in $z-$direction is $\sim 63\ \mu$m), which should mitigate numerical artifacts. Hence, the CF model is an acceptable first-order estimation of the more accurate FE model.

As mentioned above, the m material parameter is expected to be significantly different for ceramics and metals. Given that we are considering a dissimilar system, we next use a lower value for m in the metallic layer ($m_{\mathrm{Ti64}} = 3$) while leaving the SiC unchanged. As shown in Figure 2, decreasing the m should lower the normal stress and extend the axial distance at which it transitions from tensile to compressive. Furthermore, it allows for a broader distribution of the shear stress, which can be attributed to the ability to accomodate more dislocation buildup. The resulting stress components for the case of different m is shown in Figure 4. As expected, the magnitude of the peeling and shear stresses on the Ti64 layer are smaller when using the lower m parameter. Interestingly, when using different m, the shear stress develops a discontinuity at the interface which is not observed from the FE model. We also considered the Ti64/SiC configuration (see Figure 4b) which shows that the shear stress changes direction, mirroring the opposite configuration. However, the peeling stress on SiC layer is passivated at the interface, then monotonically increases deeper into the layer before going to a stress-free state away from the interface. Unlike the opposite configuration, SiC is always under a tension condition,

Table 1. Set of thermomechanical properties for the bilayered system.

Property	Material	
	SiC	Ti64
E (GPa)	434	114
ν	0.2	0.342
α (/K)	5.28×10^{-6}	9.70×10^{-6}
m	6	3
ΔT (K)	-600 (unless otherwise noted)	

a)

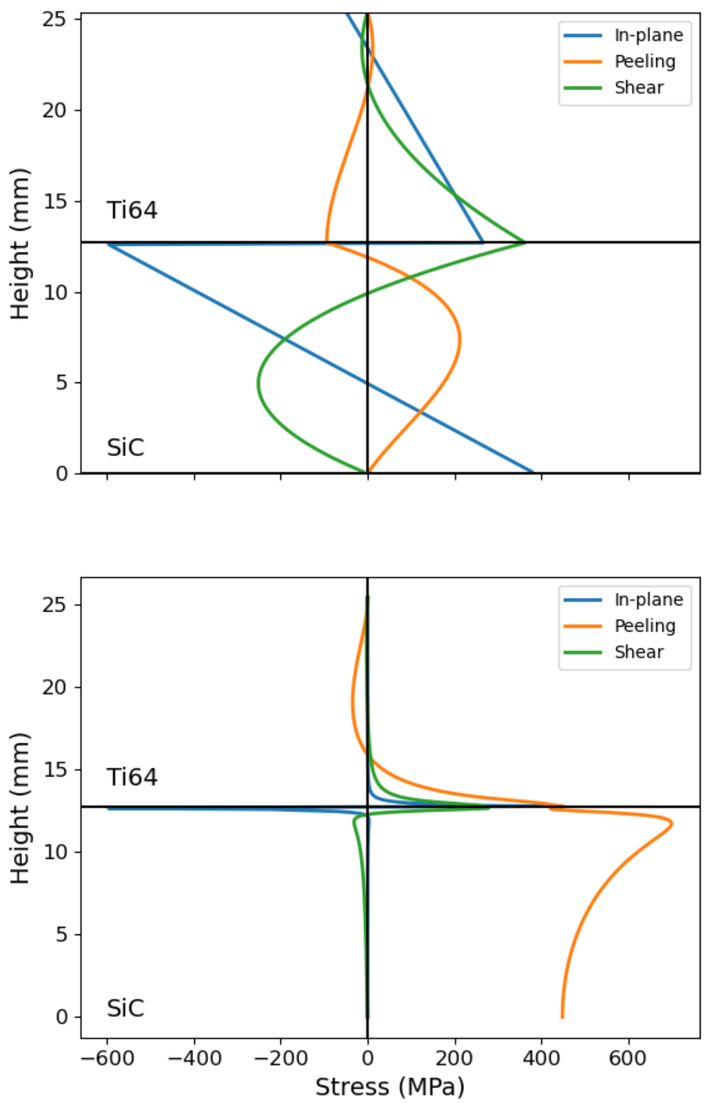

Figure 3. Different stress components near the free edge (where it is maximum) along the sample height for the a) CF (analytical) and b) FE (numerical) models.

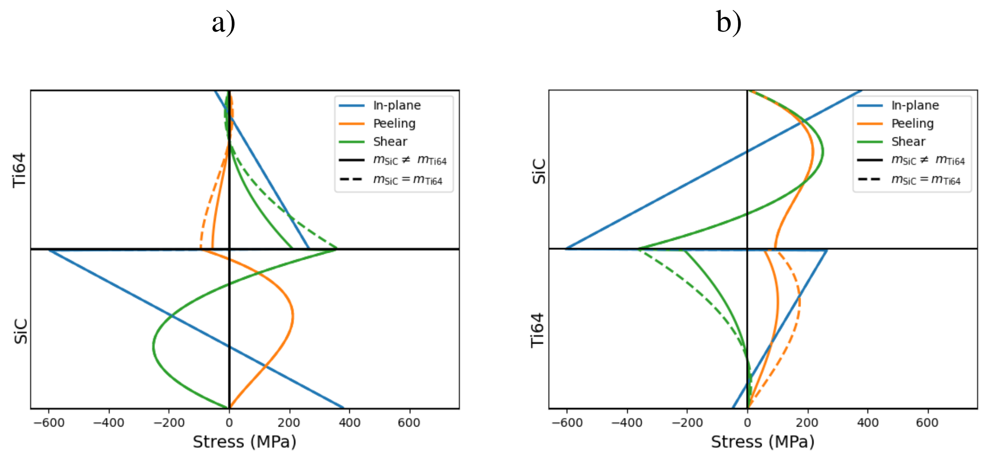

Figure 4. Influence of material-class specific m parameter on the stress components for the a) SiC/Ti64 and b) Ti64/SiC configurations. The magnitude of the peeling and shear stresses are decreased when using a smaller m.

which could correspond to a higher probability of failing via mode I delamination.

While these stress components provide a rich amount of information on the complex stress state, it is often desired to use a single metric to reduce the analysis complexity. Ceramics and metals are expected to fail via different mechanisms, fracture and plastic deformation, respectively. Therefore, we implemented both principal and von Mises stress analysis to capture the expected failure mechanisms for each constituent material. However, due to the expected mechanistic differences, we are introducing a "composite" stress analysis, which simply means that the failure analysis depends on the m parameter

$$\sigma_c = \begin{cases} \sigma_{vm}, & m \leq 3 \\ \sigma_p, & \text{otherwise} \end{cases}$$

where vm and p stand for the von Mises and principal stresses, respectively. Figure 5 shows the maximum composite, principal, and von Mises stresses across the sample thickness. As shown, the von Mises analysis is an inadequate metric for measuring failure in the ceramic layer. Using this composite stress-failure metric enables the analysis of the full system's cross section, as shown in Figure 6. As expected, we see that the maximum stresses are along the interfaces on the free edge (left side) of the samples. Of note is the large tensile stress along the SiC's base, which is likely due to the in-plane stress that dominates over the other components away from the interface.

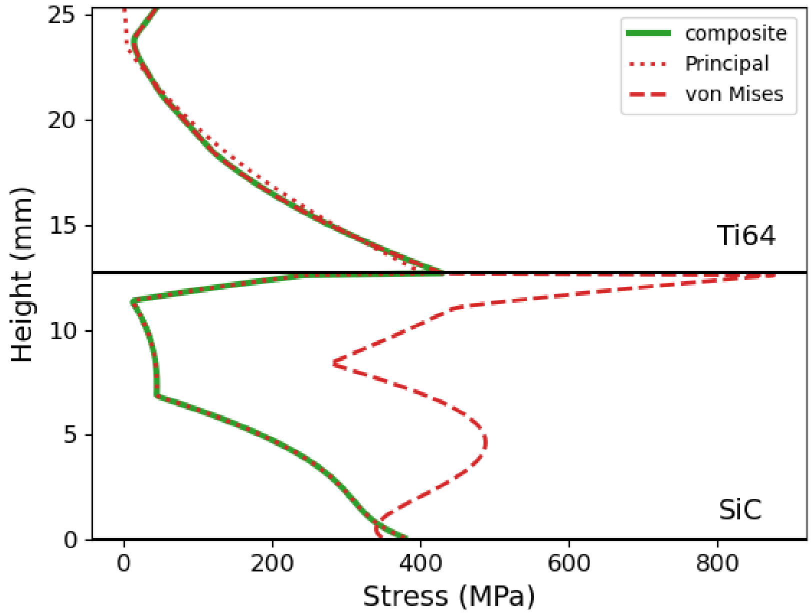

Figure 5. Comparison between principal and von Mises failure analysis for the SiC/Ti64 configuration along the free edge where stresses are maximum.

Once more we see that the principal stress analysis does reasonably well across the whole sample; however, the von Mises analysis is unable to properly capture the expected failure response in the ceramic layer.

To understand the influence of processing conditions, we looked at the effect of temperature on the maximum composite stress, shown in Figure 7. We see that the maximum stress has a linear dependence on temperature change, with a negative and positive slope for cooling ($\Delta T < 0$) and heating ($\Delta T > 0$), respectively. The highest local stresses are found to be around the interface on the SiC and Ti64 layers for heating and cooling conditions, respectively. This is due to the definition of the failure metric (composite stress field), which is directionally independent for metals (von Mises). Upon heating (expanding material), the largest stress is in a tensile state (positive stress); however, upon cooling (contracting material), the largest stress is the least compressive state (negative stress). Therefore, when undergoing cooling, the maximum stress will be the largest of the von Mises or least compressive (negative) principal stress.

To explore methods of lowering the maximum composite stress (i.e., decrease

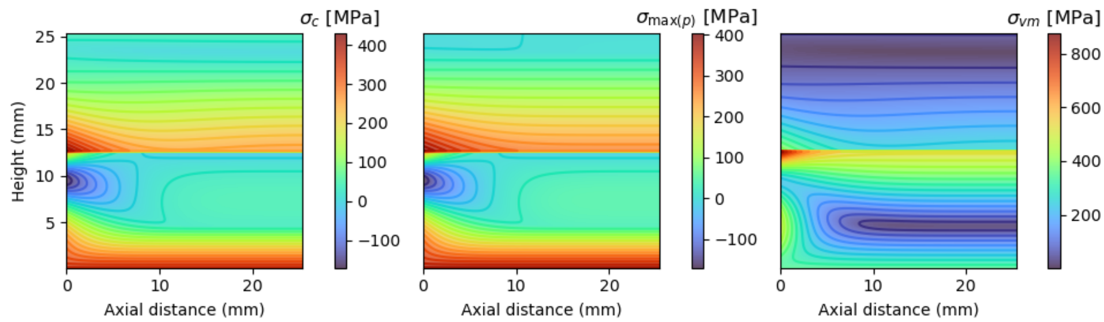

Figure 6. Comparison between principal and von Mises failure analysis for the SiC/Ti64 configuration across the cross section.

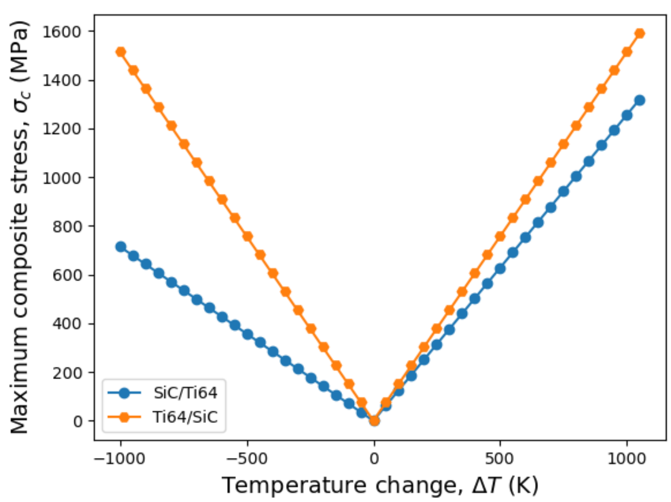

Figure 7. Maximum stress in the sample as a function of temperature.

a) b)

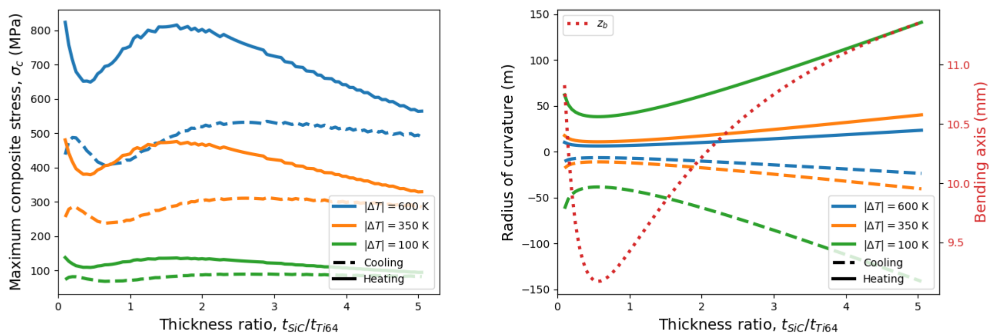

Figure 8. Influence of the thickness ratio on the a) maximum composite stress and b) radius of curvature, where the thickness of SiC varies linearly from 2.3 to 21.2 mm.

likelihood of failure), we performed a parametric study for a range of layer thickness ratios while keeping the overall sample thickness constant ($t_{\mathrm{SiC}} + t_{\mathrm{Ti64}} = 25.4$ mm). Figure 8 shows the resulting maximum stress and radius of curvature for a range of processing temperatures. The stresses are shown to vary nonlinearly for smaller SiC thicknesses ($t_{\mathrm{SiC}} < 2t_{\mathrm{Ti64}}$), followed by a linear decrease as the Ti64 layer approaches a film thickness. This is due to the complex interplay between the different strain modes. For instance, the Ti64 expands more than SiC as they are heated causing a slight compression on the ceramic layer, which is accentuated for smaller SiC thicknesses. Alternatively, as the SiC thickness increases (i.e., curvature decreases) the in-plane stress becomes dominant over the bending stress. For completeness, a map of the maximum composite stresses as a function of thickness ratio and processing temperature is shown in Figure 9.

4. Conclusion

A comprehensive analysis of the thermoelastic behavior of ceramic-metal composite systems was presented, specifically focusing on the SiC/Ti64 bilayer system, using a CF formulation extended from the Hsueh model. The study addresses the challenges posed by the mismatch in thermomechanical properties (e.g., CTE), which lead to residual stresses during thermal processing. The CF model, which provides a first-order approximation of stress states, was used to predict stress distributions, including peeling, shear, and in-plane stresses; hence, providing insights into the mechanical stability of bonded dissimilar materials under cooling and heating conditions. By comparing to an FE analysis, it was shown that the CF model captures correct stress

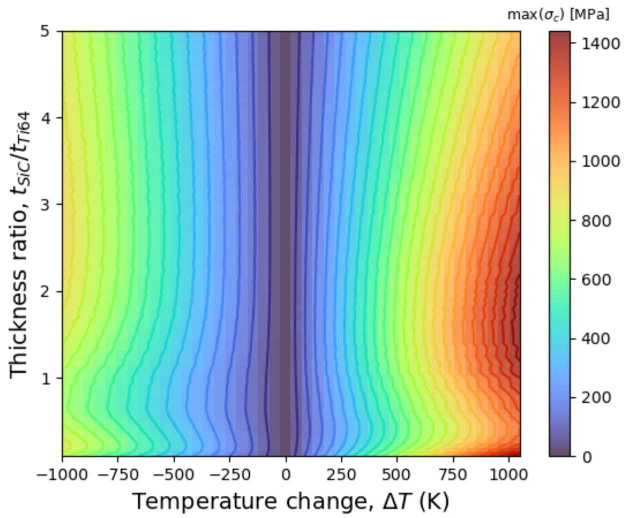

Figure 9. Map of the maximum composite stress as a function of temperature and thickness ratio. This can help determine ideal processing conditions.

directions and magnitudes at the interface, though it does not fully replicate the FE results. Nonetheless, the CF model proves useful in identifying general trends to the expected thermomechanical response, especially in regions around the interface. However, for quantitative understanding of the interlayer mechanical response, a more accurate approach (e.g., FE) should be adopted.

These stress components were used to develop a stress tensor from which a measure of mechanical damage was derived. A composite stress metric combining von Mises and principal stress analyses was introduced to account for the distinct failure mechanisms of ceramics (fracture) and metals (plastic deformation). This metric was used to analyze the bilayer system across a range of configurations to determine the highest stress state. Parametric studies reveal that the maximum stress and radius of curvature are highly sensitive to layer thickness ratios and processing temperatures, with thinner ceramic layers experiencing higher stresses due to thermal expansion mismatch.

The results emphasize the importance of optimizing layer thickness ratios and processing temperatures to minimize residual stresses and improve the mechanical performance of ceramic-metal composites. This work provides valuable guidance for designing and processing advanced material systems for high-temperature applications.

5. References

1. Marshall D et al. National Hypersonic Science Center for Materials and Structures. Air Force Office of Scientific Research (US); 2014.
2. Jung YI et al. Effect of Ti and Si interlayer materials on the joining of SiC ceramics. Nuclear Engineering and Technology. 2016;48:1009–1014.
3. Jung YI, Kim SH, Kim HG, Park JY, Kim WJ. Microstructures of diffusion bonded SiC ceramics using Ti and Mo interlayers. Journal of Nuclear Materials. 2013;441:510–513.
4. Henager CH Jr et al. Coatings and joining for SiC and SiC-composites for nuclear energy systems. Journal of Nuclear Materials. 2007;367:1139–1143.
5. Liu Y, Huang Z, Liu X. Joining of sintered silicon carbide using ternary Ag–Cu–Ti active brazing alloy. Ceramics International. 2009;35:3479–3484.
6. Akselsen O. Advances in brazing of ceramics. Journal of Materials Science. 1992;27:1989–2000.
7. Timoshenko S. Analysis of bi-metal thermostats. Journal of the Optical Society of America. 1925;11:233–255.
8. Hu S. Stress-related problems in silicon technology. Journal of Applied Physics. 1991;70:R53–R80.
9. Hsueh CH. Thermal stresses in elastic multilayer systems. Thin Solid Films. 2002;418:182–188.
10. Hsueh CH, Luttrell CR, Cui T. Thermal stress analyses of multilayered films on substrates and cantilever beams for micro sensors and actuators. Journal of Micromechanics and Microengineering. 2006;16:2509.
11. Hsueh CH, Luttrell CR, Lee S, Wu TC, Lin HY. Interfacial peeling moments and shear forces at free edges of multilayers subjected to thermal stresses. Journal of the American Ceramic Society. 2006;89:1632–1638.
12. Hsueh CH. Delamination at free edges. Springer; 2014. p. 890–901.
13. Bao Y, Su S, Huang JL. An uneven strain model for analysis of residual stress and interface stress in laminate composites. Journal of Composite Materials. 2002;36:1769–1778.
14. Pelz J et al. Gradient ceramic structures via multi-material direct ink writing. Applied Materials Today. 2024;40:102366.

Appendix. Derivation of Bending and Shear Momentum

The Hsueh[1] and Bao[2] formulations assume different axis, i.e., flipped in reference to each other. To properly define the required momentum closed forms, we carefully derived these by integrating the forms outlined by the respective models.

For the bending moment, starting with Equation 4 from Hsueh's formulation, we can separate the integral to be defined internally ($\{\mathrm{T}_i \in \mathbb{R} : h_{k-1} \leq z \leq h_k\}$) and externally ($\{\mathrm{T}_i \in \mathbb{R} : h_{k+1} \leq z \leq h_n\}$)

$$\begin{aligned} M_k &= -\sum_{i=k}^{n} \int_{h_{i-1}}^{h_i} \sigma_i \cdot (z - h_{k-1}) dz \\ &= -\left[\int_{h_{k-1}}^{h_k} \sigma_k \cdot (z - h_{k-1}) dz + \sum_{i=k+1}^{n} \int_{h_{i-1}}^{h_i} \sigma_i \cdot (z - h_{k-1}) dz \right] \end{aligned} \tag{A.1}$$

Inserting Hsueh's in-plane stress definition into Equation A.1 and applying integration by parts, we get

$$-E_k \int_{h_{k-1}}^{h_k} \left(\varepsilon_u + \frac{z - z_b}{\mathcal{R}} - \alpha_k \Delta T \right) \cdot (z - h_{k-1}) dz$$

$$\begin{aligned} u &= \varepsilon_u + \frac{z - z_b}{\mathcal{R}} - \alpha_k \Delta T & dv &= (z - h_{k-1}) dz \\ du &= \frac{1}{\mathcal{R}} dz & v &= \frac{(z - h_{k-1})^2}{2} \end{aligned}$$

$$\left(\varepsilon_u + \frac{z - z_b}{\mathcal{R}} - \alpha_k \Delta T \right) \frac{(z - h_{k-1})^2}{2} \Bigg|_{h_{k-1}}^{h_k} - \int_{h_{k-1}}^{h_k} \frac{(z - h_{k-1})^2}{2\mathcal{R}} dz,$$

resulting in

$$F = -E_k \left[\left(\varepsilon_u + \frac{z - z_b}{\mathcal{R}} - \alpha_k \Delta T \right) \frac{(z - h_{k-1})^2}{2} - \frac{(z - h_{k-1})^3}{6\mathcal{R}} \right] \Bigg|_{z}^{h'_k} \tag{A.2}$$

This form is used to calculate the k^{th} inter-layer ($[z, h_k]$) bending moment

[1] Hsueh CH. Delamination at free edges. Springer; 2014. p. 890-901.

[2] Bao Y, Su S, Huang JL. An uneven strain model for analysis of residual stress and interface stress in laminate composites. Journal of Composite Materials. 2002;36:1769–1778.

$$M_i(z) = -E_k\Big[\left(\varepsilon_u + \frac{h_i - z_b}{\mathcal{R}} - \alpha_i \Delta T\right)\frac{t_i^2}{2} - \frac{t_i^3}{6\mathcal{R}} \\ - \left(\varepsilon_u + \frac{z - z_b}{\mathcal{R}} - \alpha_i \Delta T\right)\frac{(z - h_{i-1})^2}{2} + \frac{(z-h_{i-1})^3}{6\mathcal{R}}\Big], \tag{A.3}$$

yielding a closed form for every discretized height within the layer. To account for the contributions from subsequent layers $(k+1, n)$, we consider the height of interest (z) to a virtual interface at which peeling moment and shear force are in equilibrium with those induced by the imaginary applied traction. Then, evaluating for the j^{th} extralayer ($[h_{j-1}, h_j]$), we get

$$M_j(z) = -E_j\Big[\left(\varepsilon_u + \frac{h_j - z_b}{\mathcal{R}} - \alpha_j \Delta T\right)\frac{(h_j - z)^2}{2} - \frac{(h_j - z)^3}{6\mathcal{R}} \\ - \left(\varepsilon_u + \frac{h_{j-1} - z_b}{\mathcal{R}} - \alpha_j \Delta T\right)\frac{(h_{j-1} - z)^2}{2} + \frac{(h_{j-1}-z)^3}{6\mathcal{R}}\Big]. \tag{A.4}$$

Finally, to get the total bending moment for the k^{th} layer across different thickness heights, we get

$$M_k(z) = M_i(z) + \sum_{j=i+1}^{n} M_j(z). \tag{A.5}$$

As outlined in the report, we now use the formulation by Bao to determine the stress state across the layer's cross section; however, the frame of reference needs to be flipped to agree with Hsueh's

$$M_{k,\max} = \int \sigma \cdot x dx = D \int_0^{x_0} \left[(L-x)^{m-1} - (L-x_t)^{m-1}\right] \cdot \; x dx. \tag{A.6}$$

Integrating by parts and simplifying, we get

$$\begin{aligned} u &= x & dv &= (L-x)^{m-1} - (L-x_t)^{m-1} \\ du &= dx & v &= -\frac{(L-x)^m}{m} - (L-x_t)^{m-1}x \end{aligned}$$

$$-x\left[\frac{(L-x)^m}{m}+(L-x_t)^{m-1}x\right]+\int\frac{(L-x)^m}{m}+(L-x_t)^{m-1}x\,dx$$

$$-x\left[\frac{(L-x)^m}{m}+(L-x_t)^{m-1}x\right]-\frac{(L-x)^{m+1}}{m(m+1)}+(L-x_t)^{m-1}\frac{x^2}{2}$$

$$-\frac{2(L-x)^m\cdot(L+mx)+m(m+1)\cdot(L-x_t)^{m-1}x^2}{2m(m+1)}$$

Evaluating at integral bounds $(0, x_0)$, we get

$$M_{k,\max}(x)=-D\frac{2(L-x_0)^m\cdot(L+mx_0)+m(m+1)\cdot(L-x_t)^{m-1}x_0^2-2L^{m+1}}{2m(m+1)}. \tag{A.7}$$

Finally, we can get a closed form for the stress state by combining the bending moment formulations (Equations A.5 and A.7)

$$\sigma=-\frac{2m(m+1)M_k(z)\left((L-x)^{m-1}-(L-x_t)^{m-1}\right)}{2(L-x_0)^m\cdot(L+mx_0)+m(m+1)\cdot(L-x_t)^{m-1}x_0^2-2L^{m+1}}. \tag{A.8}$$

List of Symbols, Abbreviations, and Acronyms

α	Coefficient of Thermal Expansion
ε_b	bending strain component
ε_{th}	thermal strain component
ε_u	uniform strain component
σ	stress state
τ	shear stress
E	Young's modulus
M	peeling moment per unit length
$\mathcal{R}$	radius of curvature
V	shear force per unit length
T	processing temperature
T_0	reference temperature
h	layer top height
t	layer thickness
z	domain height
z_b	bending axis
Al	Aluminum
C	Carbon
CCC	Carbon-Carbon Composite
CF	Closed-Form
CMC	Ceramic Matrix Composite
CTE	Coefficient of Thermal Expansion
MCC	Metallic Ceramic Composite
FE	Finite Element
Si	Silicon
SiC	Silicon Carbide
Ti	Titanium

TiC	Titanium Carbide
Ti64	Ti-6Al-4V
V	Vanadium

1	DEFENSE TECHNICAL
(PDF)	INFORMATION CTR
	DTIC OCA
1	DEVCOM ARL
(PDF)	FCDD RLD DCI
	TECH LIB